### 8

#### Research Article

Shao-Hsuan Wu and Jun-Hui Huang\*

# Two mixed-ligand coordination polymers based on 2,5-thiophenedicarboxylic acid and flexible N-donor ligands: the protective effect on periodontitis via reducing the release of IL-1 $\beta$ and TNF- $\alpha$

https://doi.org/10.1515/chem-2020-0081 received January 31, 2020; accepted March 17, 2020

Abstract: Two novel mixed-ligand coordination polymers,  $\{[Co(tdc)(btrp)]\cdot 0.67DMF\}_n$  (1) and  $\{[Zn_2(bimb)_2(tdc)_2]\cdot (Dn_2(bimb)_2(tdc)_2)\}$  $2H_2O_n$  (2) involving 2,5-thiophenedicarboxylate ( $H_2tdc$ ), and bitopic flexible N-donor ligands, 1,3-bis(1,2,4-triazol-1-yl)propane (btrp) and 1,4-bis((1*H*-benzo[*d*]imidazol-1-yl)methyl)benzene (bimb), have been synthesized by the hydrothermal method and characterized via IR, elemental analysis, thermal analysis, and powder X-ray diffraction. The biological functional studies were performed; the treatment activity of the compounds on periodontitis and the specific mechanism was explored. First, the real-time RT-PCR was carried out to determine the inflammatory genes nf-kb and p53 relative expression in periodontal mucosal cells after treating with compounds 1 and 2. Then, the level of the inflammatory cytokine in the gingival crevicular fluid after treating with compounds was also determined by the ELISA detection kit.

**Keywords:** coordination polymer, mixed-ligand, X-ray diffraction, periodontitis

### 1 Introduction

Periodontitis is one of the most common oral diseases worldwide. Studies have shown that the invaded pathogens could adhere to the gums and periodontal tissues, multiply, grow, and the metabolic substance produced by the invaded pathogens can activate the immune system, causing edema and bleeding of soft

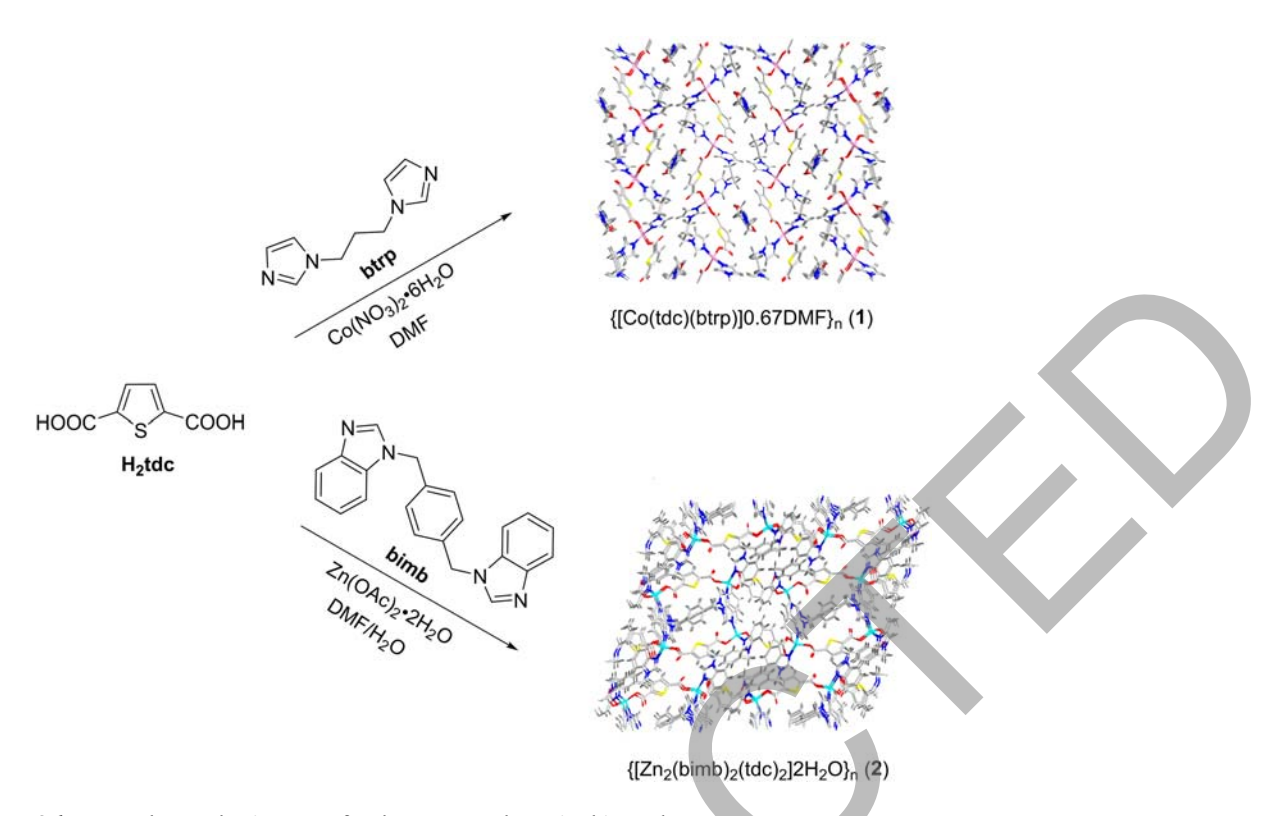
tissue, and formation of periodontal pockets [1,2]. The biggest hidden danger of periodontitis is that periodontitis can induce other systems disease. According to related researches, periodontitis has a certain correlation with the occurrence of diabetes and cardiovascular diseases, and it has a potential and profound threat to human health [3].

In recent years, the design and synthesis of coordination polymers (CPs) have attracted much attention due to their fascinating molecular topologies and potential applications in catalysis, molecular detection, microelectronics, ion exchange, and nonlinear optics [4-7]. In general, the structural diversity of these crystal materials is decided by many factors such as counterions, templates, metal coordination ratio, metal ions, the value of pH, and the coordination of organic ligands [8-10]. In these specific strategies, the reasonable selection of the functional group, rigidity, and length of co-ligand or organic ligand is very significant for structure-controlled CPs assembly, and many important works have been completed via utilizing this strategy [11-13]. In general, organic ligands with curved skeletons, for example, quadrilateral, triangular, and V-shaped, are ideal for the construction of interpenetrating, highly connected, or helical coordination systems because of their versatile bridging methods and curved skeletons. In addition, the carboxylic acid groups are the good hydrogen-bond donor and hydrogen-bond acceptor, which are decided by the deprotonation degree. Among these, 3,3',4,4'benzophenone tetracarboxylic acid, 1,2,4,5-benzenetetracarboxylic acid, 2,5-thiophene-dicarboxylic acid, 4,4'-oxydibenzoic acid, and other quadrangular polycarboxylic acids have attracted much attention because of their rich coordination patterns [14–16]. In addition to carboxylic acid linkers, flexible bisimidazole and its derivatives have multiconformation and strong coordination ability, which can be utilized as the auxiliary ligands in order to construct fascinating metal CPs [17]. Hence, in this research, two novel mixed-ligand coordination polymers,  $\{[Co(tdc)(btrp)]\cdot 0.67DMF\}_n$  (1) and  $\{[Zn_2(bimb)_2(tdc)_2]\cdot 2H_2O\}_n$  (2)

**Shao-Hsuan Wu:** Xiangya Stomatological Hospital, Central South University, Changsha, Hunan, China

<sup>\*</sup> Corresponding author: Jun-Hui Huang, Xiangya Stomatological Hospital, Central South University, Changsha, Hunan, China, e-mail: Junhui\_huang11@126.com

<sup>∂</sup> Open Access. © 2020 Shao-Hsuan Wu and Jun-Hui Huang, published by De Gruyter. © This work is licensed under the Creative Commons Attribution 4.0 Public License.



Scheme 1: The synthesis routes for the two complexes in this work.

involving 2,5-thiophenedicarboxylate (H2tdc), and bitopic flexible N-donor ligands, 1,3-bis(1,2,4-triazol-1-yl)propane (btrp) and 1,4-bis((1*H*-benzo[*d*]imidazol-1-yl)methyl)benzene (bimb), have been synthesized by hydrothermal method and characterized via IR, elemental analysis, thermal analysis, and powder X-ray diffraction (Scheme 1). In the biological research, the treatment activity of compounds 1 and 2 on periodontitis was evaluated, and the related mechanism was revealed. First, the results of the real-time RT-PCR demonstrated that compound 1 revealed a much stronger inhibitory function on the inflammatory genes  $nf-\kappa b$  and p53relative expression level in periodontal mucosal cells than compound 2. Besides, the ELISA data of the inflammatory cytokines' level in the gingival crevicular fluid also indicated that the anti-inflammatory effect of compound 1 is better than that of compound 2.

## 2 Experimental

#### 2.1 Chemicals and measurements

All chemicals were purchased from the market and utilized with no extra purification. The analyses of

element (N, H, and C) were carried out with the PerkinElmer 240C analyzer. The infrared spectrum between 4,000 and 400 cm<sup>-1</sup> was recorded on the Bruker Alpha spectrometer using pure solid samples. The data of powder X-ray diffraction (PXRD) with the Bruker D8-ADVANCE X-ray diffractometer were collected using Cu K $\alpha$  radiation ( $\lambda$  = 1.5418 Å) in 2 $\theta$  range 5–50°. Thermogravimetric analyses were performed with the Labsys Evo thermal analyzer at 25–800°C in the nitrogen atmosphere, and the heating rate was 5°C min<sup>-1</sup>.

# 2.2 Preparation and characterization for $\{[Co(tdc)(btrp)]\cdot 0.67DMF\}_n$ (1) and $\{[Zn_2(bimb)_2(tdc)_2]\cdot 2H_2O\}_n$ (2)

For complex **1**, the solution of  $Co(NO_3)_2$ · $6H_2O$  (0.5 mmol, 1.0 M, 0.5 ml in DMF) was added into a glass bottle containing btrp ligand (89.1 mg and 0.5 mmol) and 1.25 ml of 0.4 M  $H_2$ tdc (0.5 mmol mixture in DMF). The obtained mixture was stirred at the ambient temperature for a few minutes until all the reagents are completely dissolved. The vial was placed in the oven for half a day at 95°C. Then, the bottle was removed from the oven and

then cooled it to the ambient temperature. Pink blockshaped crystals were formed at the bottom. The crystals were washed for twice with 2 ml DMF and then stored in a glass bottle under DMF. The yield was approximately 100 mg (ca. 42%) based on the  $H_2$ tdc ligand. Elemental analysis: found, %: C 45.19, H 4.22, N 12.83 and calculated ([Co(btrp)(tdc)]·0.67DMF), %: C, 44.97; H, 4.14; Co, 12.98; N, 14.40. IR bands, cm<sup>-1</sup>: 3,125 m, 2,934 m, 1,668 s, 1,630 s, 1,590 m, 1,531 m, 1,461 s, 1,353 s, 1,280 m, 1,209 m, 1,173 s, 1,128 m, 995 w, 899 s, 812 m, 769 m, 677 m.

For complex **2**,  $Zn(OAc)_2 ext{-}2H_2O$  (0.2 mmol and 43.8 mg),  $H_2tdc$  (0.1 mmol and 17.0 mg), bimb (0.1 mmol, 34 mg), DMF (5 ml), and  $H_2O$  (2 ml) were mixed in a 25 ml Telfon-lined stainless steel vessel to form a mixture, heated at 140°C for 72 h under spontaneous pressure, and then cooled to the room temperature at the rate of 5°C/h. Colorless block-shaped single crystals were obtained. The yield was 42.3% based on bimb. Calc. For  $1(C_{60}H_{52}N_8O_{10}S_2Zn_2)$ : C, 58.12; H, 4.23; N, 9.04%. Found: C 57.28, H 4.40, N 9.14%. IR (KBr, cm<sup>-1</sup>): 3,426 s, 1,614 s, 1,527 m, 1,459 m, 1,411 m, 1,343 s, 751 s.

X-ray data were calculated using an Oxford XcaliburE diffractometer. CrysAlisPro software was used to analyze the intensity data and convert them into HKL files. The direct method with SHELXS program was used to establish the initial structure model of compound 1 and modified using least square means with SHELXL-2014 program. All the non-H atoms of complex 1 were refined with anisotropic parameters. Then, all the H atom by using AFIX command to geometrically fix on the C atom they are linked to. The crystallographic parameters and the refinement of these two complexes were listed in Table 1.

#### 2.3 Real-time RT-PCR

In order to determine the inhibitory effect of the compounds 1 and 2 on the inflammatory genes nf- $\kappa b$  and p53 relative expression level in periodontal mucosal cells, the reverse transcription-polymerase chain reaction (RT-PCR) was carried out to detect nf- $\kappa b$  and p53 relative expression. This experiment was conducted with instructions construction. In brief, the periodontitis animal model was established, compounds 1 and 2 were given for indicated treatment with 5 mg/kg via i.p, and ligands and ions were used as control compounds. The periodontal mucosal cells were harvested and cleaned, and total RNA was within cells by TRIzol reagent following the instruction of the manufacturer. The OD260/OD280 ratio was used to determine the total RNA concentration, and total RNA was reverse

**Table 1:** Refinement details and crystallographic parameters for complexes 1 and 2

Identification code	1	2
Empirical formula	$C_{33}H_{35}Co_2N_9O_9S_2$	$C_{60}H_{48}N_8O_8S_2Zn_2$
Formula weight	883.68	1203.92
Temperature/K	296.15	296.15
Crystal system	Monoclinic	Triclinic
Space group	P2 <sub>1</sub> /c	PĪ
a/Å	6.23690(10)	11.3621(14)
b/Å	15.2236(4)	14.987(2)
c/Å	18.9365(5)	18.963(2)
α/°	90	103.554(4)
β/°	90.522(2)	107.1360(10)
γ/°	90	101.3890(10)
Volume/Å <sup>3</sup>	1797.91(7)	2873.8(6)
Z	2	2
$ ho_{\rm calc} \ {\rm g/cm^3}$	1.632	1.391
$\mu/\text{mm}^{-1}$	1.107	0.969
Data/restraints/parameters	3,640/38/249	11,478/0/685
Goodness-of-fit on F <sup>2</sup>	1.050	0.974
Final $R$ indexes $[I \ge 2\sigma(I)]$	$R_1 = 0.0482$ ,	$R_1 = 0.0646$ ,
	$\omega R_2 = 0.1539$	$\omega R_2 = 0.1743$
Final R indexes [all data]	$R_1 = 0.0505,$	$R_1 = 0.1213,$
	$\omega R_2 = 0.1564$	$\omega R_2 = 0.2093$
Largest diff. peak/hole/e ${\rm \AA}^{-3}$	0.89/-0.75	0.78/-0.68
CCDC	1981070	1981071

transcripted into cDNA by a high-capacity cDNA reverse transcription kit. Ultimately, the nf- $\kappa b$  and p53 relative expression levels in periodontal mucosal cells were determined by SYBR Green Master Mix after compound treatment. The  $2^{-\Delta\Delta Ct}$  method was used for relative quantification from triplicate preformation. The primers sequences utilized in this experiment were summed up in Table 2.

Table 2: The primers sequences utilized in this study

Genes	Sequences
nf-кb	CCACCCGGCTTCAGAATGG
	AACCTTTGCTGGTCCCACAT
p53	TGCTCAAGACTGGCGCTAAA
	GCTCGACGCTAGGATCTGAC
gapdh	AATGGGCAGCCGTTAGGAAA
	GCGCCCAATACGACCAAATC

#### 2.4 ELISA detection

After treated by compounds 1 and 2, TNF- $\alpha$  and IL-1 $\beta$  contents in the gingival crevicular fluid were detected by ELISA. This preformation was carried out in accordance with the manufactures' protocols. Briefly, the periodontitis rat model was constructed, and 5 mg/kg of

compound 1 or 2 was given for the indicated treatment. Then, the gingival crevicular fluid was collected from all the groups, followed by the IL-1 $\beta$  and TNF- $\alpha$  content determination with the ELISA detection kit. This experiment was carried out three times, and the results were expressed as mean  $\pm$  standard deviation.

**Ethical approval:** The conducted research is not related to either human or animal use.

#### 3 Results and discussion

#### 3.1 Molecular structure

The targeted complex **1** could be obtained through the reaction of  $Co(NO_3)_2$ · $6H_2O$  with  $H_2$ tdc btrp in the solution of DMF for half a day, whose chemical formula was established to be  $\{[Co(tdc)(btrp)]\cdot 0.67DMF\}_n$  on the basis of the diffraction for single-crystal X-ray and the analysis for element along with the TGA curve. According to the crystal data that were collected under the ambient temperature, the results of the structural solution along with refinement reveal that complex **1** is part of the system of monoclinic crystal with a  $P2_1/c$  space group and has a two-dimensional layered structure. In the

fundamental molecular repeating unit, there is a crystallography absolute Co(II) ion, a completely deprotonated ligand tdc<sup>2-</sup>, two-third DMF, and a ligand btrp (Figure 1a). The Co(II) center coordination surroundings are composed of two carboxylic acid oxygen atoms of two distinct ligands tdc<sup>2-</sup> and two nitrogen atoms of two ligand btrp, shaping a CoN<sub>2</sub>O<sub>2</sub>-distorted tetrahedral geometry. The Co-O bond distance is between 1.890(3) and 1.946(3) Å, and the Co-N bond length is between 1.960(3) and 1.946(3) Å. The ligands of tdc<sup>2-</sup> and btrp alternate along the axis a and axis b chains, which contribute to the 2D-layered network (Figure 1b). The entire layer is arranged along plane *ab* (Figure 1c). Among the layer, the Co atoms deviate 0.55 Å from their average plane. The dicarboxylic acid ligand in complex 1 uses the  $\mu$ - $0^{2-}$  coordination pattern, exhibiting pairs of short (1.93, 1.98 Å) distances of Co...O. Complex 1 reveals a two-layer interpenetration in which each Co node of each array is located below or above the approximate center of the other layer space. Because of interpenetration, only individual voids filled via the DMF molecules are shown, and solvents can enter the volume (about 22%). Each hole involves a DMF molecule, which is disturbed via two positions because of its proximity to the inversion center (Figure 1d).

Complex **2** crystallizes in the triclinic  $P\overline{1}$  space group. The asymmetric unit consisted of two zinc(II) centers and two ligands of bimb and  $tdc^{2-}$  (Figure 2a).

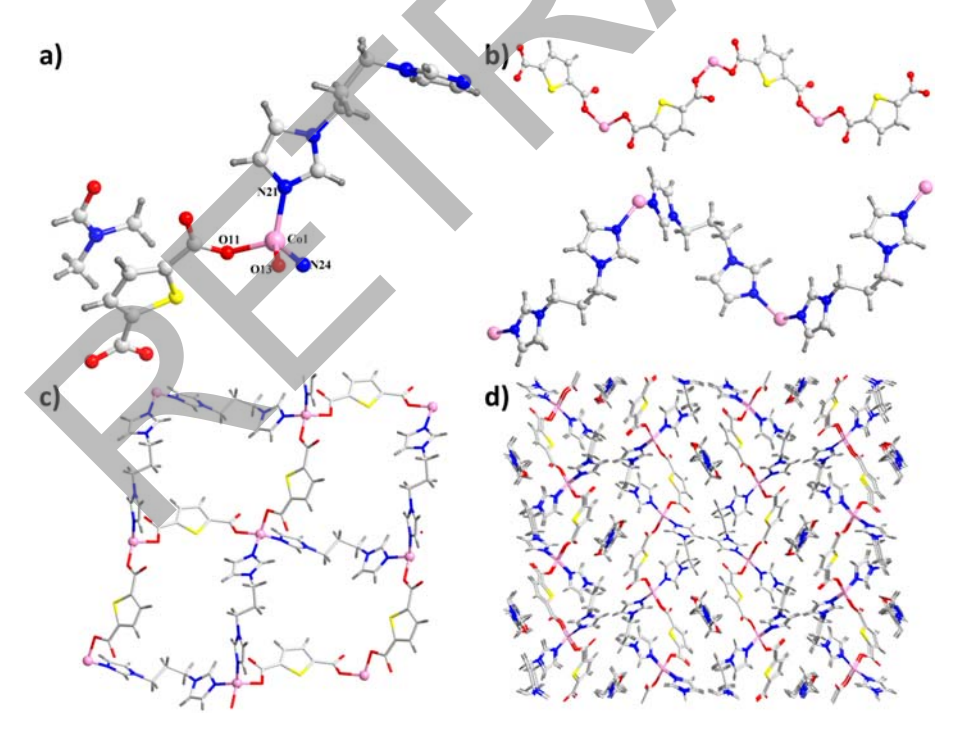


Figure 1: (a) View for the coordination surrounding of Co(II) ion in complex 1. (b) The coordination patterns for the two ligands in 1. (c) 1's two-dimensional layered network. (d) The packing diagram of 1 showing the voids that occupied via the DMF molecules.

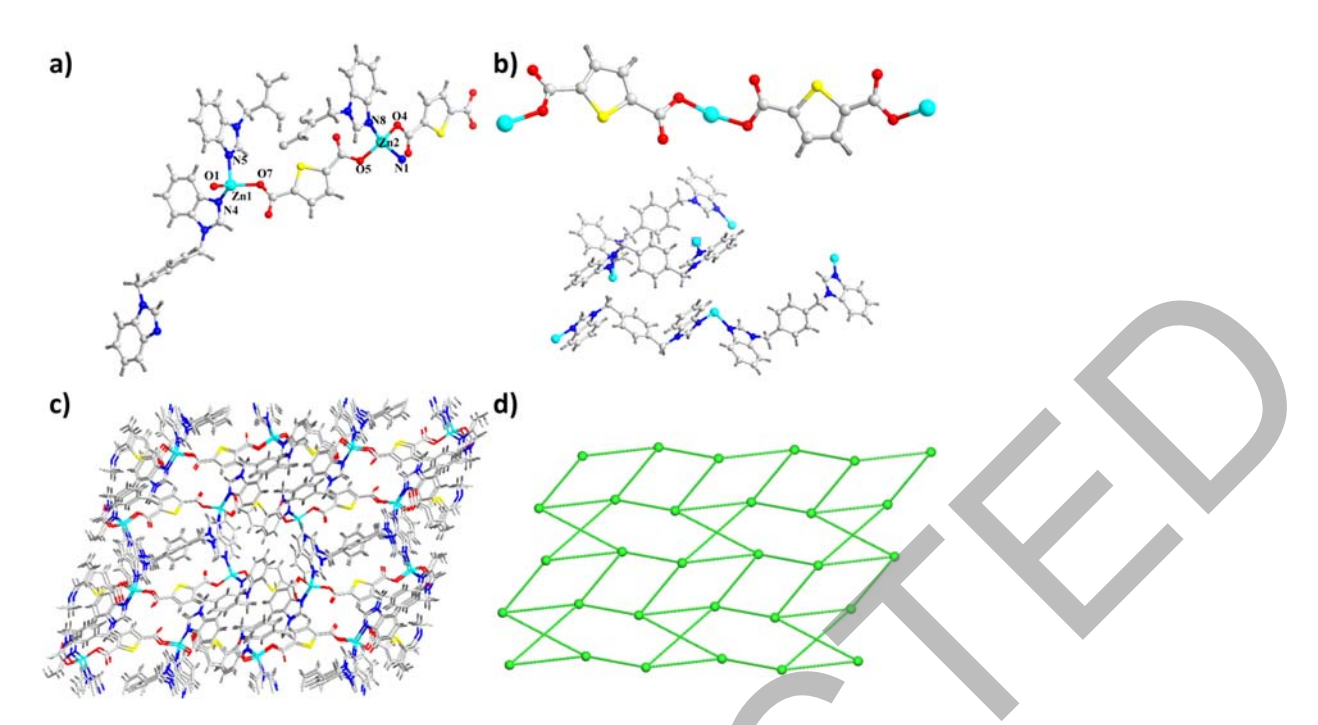


Figure 2: (a) View for an asymmetric unit for complex 2. (b) These two ligands' coordination modes. (c) 2's three-dimensional skeleton. (d) The sra topology for complex 2.

Both Zn1 and Zn2 are four-coordinated in the tetrahedron surroundings. Zn1 is coordinated via two N atoms (N5 and N4) of two distinct ligands bimb and two O atoms (O1A and O7, the symmetry code is A = 2 - x, 1 - y, 1 - z) of two absolute  $tdc^{2-}$  connectors; Zn2 is coordinated via two N atoms (N1B and N8, the symmetry code is B = 1 + x, y, 1 + z) of two separate ligands of bimb and two diverse O atoms (O5 and O4) of two ligands tdc2-; the Zn-O bond distance is between 1.916(4) and 1.956(4) Å, while the Zn-N bond distance is between 2.011(4) and 2.046(5) Å. All of these bond lengths are between the expected ranges. In complex 2, the ligands tdc<sup>2-</sup> are completely deprotonated, and the coordination pattern of  $(\kappa_1 - \kappa_0) - (\kappa_1 - \kappa_0) - \mu_2$  is used to connect the adjacent centers of Zn(II) to generate a one-dimensional infinite wave-like chain, and the contiguous Zn...Zn distance was 10.366(2) Å, and the bond angle of Zn···Zn···Zn is 131.45(8)° (Figure 2b). The ligands of bimb, which were used as  $\mu_2$  connectors, utilize the conformation of alternating cis-coordinated and transcoordinated to construct a one-dimensional "ladder"like chain, and the Zn...Zn bond distance is between 11.859 (2) and 13.745 (2) Å. The dihedral angles of two benzimidazole rings for two absolute ligands of bimb are 83.32(5) and 85.49(4)°. In addition, the one-dimensional trapezoid chain intersects the one-dimensional waveform chain vertically via sharing the Zn(II) centers, forming a complex three-dimensional skeleton (Figure 2c).

The analysis of topology was carried out through the program package ToposPro. The Zn center linked via two ligands of bimb and  $tdc^{2-}$  can be considered as a 4-linked node, the network has a special **sra** topology, and its point symbol is  $\{4^2,6^3,8\}$  (Figure 2d).

In order to determine these complexes regarding the phase purity, powder X-ray diffraction (PXRD) experiments were carried out (Figure 3a). The simulated and experimental PXRD peak positions are consistent, which shows that the crystal structures are the real representative of the bulk crystal. The strength difference may be due to the crystal samples' preferred orientation. Meanwhile, in order to study 1's and 2's thermal stability, the experiment thermogravimetric analysis (TGA) was performed between 25 and 800°C with the reflux of nitrogen, and the heating rate is 10°C min<sup>-1</sup> (Figure 3a). Complex 1 reveals the TG curve with two weight loss steps: the first weight loss of 10.9% from room temperature until the 240°C temperature, which could be related to the removal of the lattice DMF molecule (calcd: 10.7%), and the second weight loss of 41.4% begins from approximately 250°C and continues to approximately 500°C, indicating the decomposition of the btrp ligand (calcd: 38.9%). The residual powders could be assigned to the Co-tdc complex, which might be further decomposed above the temperature of 600°C. For complex 2's curve of TGA, the main weight loss possesses three distinct steps: the first weight loss occurred from 38 to 95°C, which is due to the

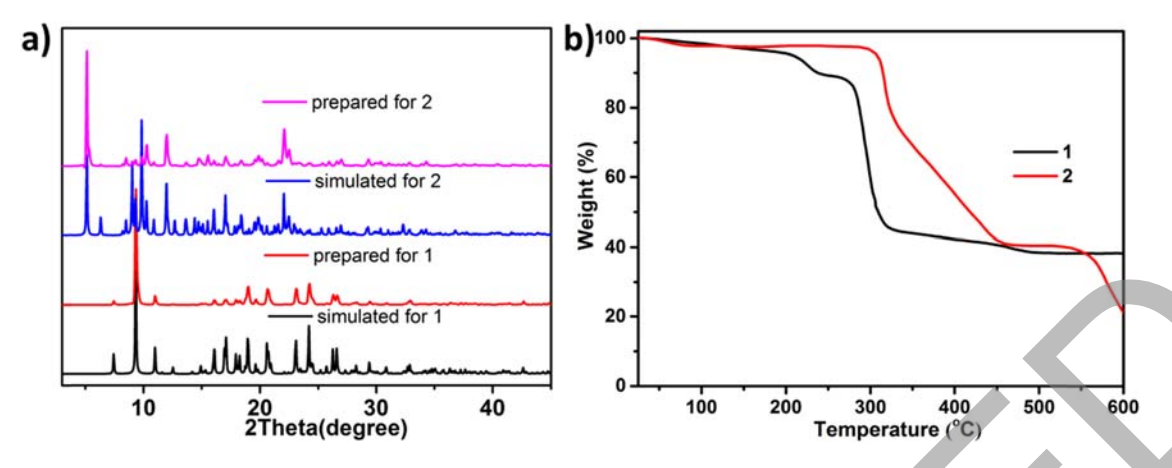


Figure 3: (a) Complexes 1's and 2's PXRD diagrams. (b) Complexes 1's and 2's curves of TGA.

removal of two lattice water molecules (found: 3.4%, calcd 2.9%); the second weight loss of 56.2% can attribute to the decomposition of bimb ligands at the range of 300 to 452°C (calcd: 54.7%); and the third weight loss from 556 to 600°C could be due to the release of the tdc²-ligand. Due to the low-temperature range of the TGA curve, a higher weight loss of complex **2** might be expected at a higher temperature.

# 3.2 Compound reduced the expression level of inflammatory genes *nf-κb* and *p53* in periodontal mucosal cells

In the process of periodontitis, there was generally an increased level of the inflammatory response in

periodontal mucosal cells, reflected as the increased expression level of the inflammatory genes  $nf-\kappa b$  and p53. Therefore, in this study, the real-time RT-PCR was carried out in order to measure the inflammatory genes nf-xb and p53 expression level in periodontal mucosal cells after treated by compounds 1 and 2. According to the result shown in Figure 4, the levels of p53 and nf-κb were increased in the groups model when compared with the group of control. After compound 1 treatment, the inflammatory response in periodontal mucosal cells was significantly relied. However, compound 2 has almost no effect on the level of inflammatory response, which revealed that compound 1 has a stronger inhibitory function against the inflammatory response in periodontal mucosal cells than compound 2. In addition, the related ligands and ions showed no effect on the gene expression.

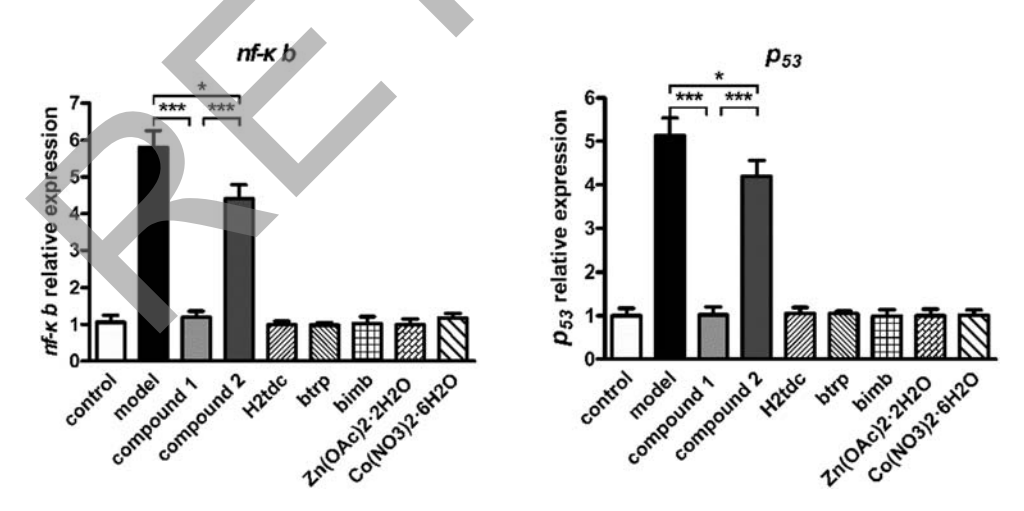


Figure 4: Reduced the expression level of inflammatory genes nf- $\kappa b$  and p53 in periodontal mucosal cells. The periodontitis rat model was constructed, and then treated by compounds 1 and 2 at the concentration of 5 mg/kg. The expression level of inflammatory genes nf- $\kappa b$  and p53 in periodontal mucosal cells was measured with real-time RT-PCR.

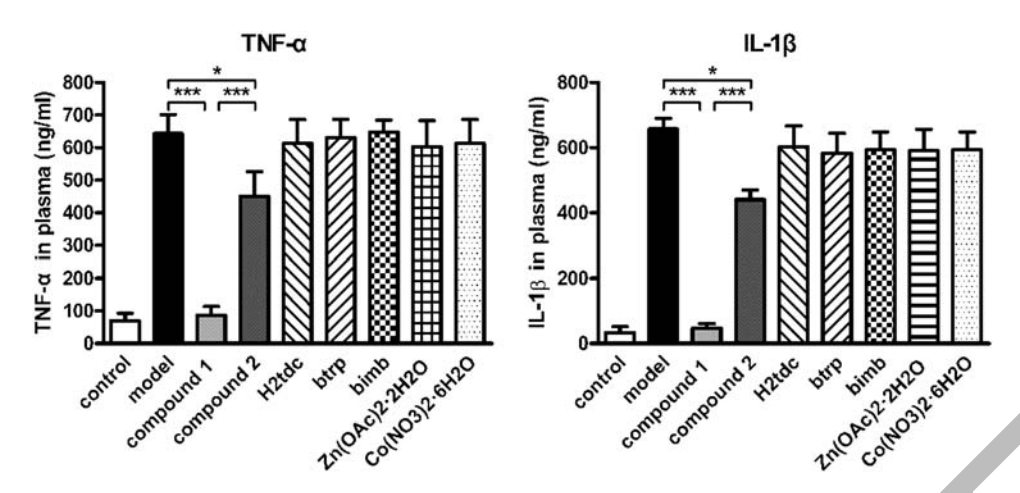


Figure 5: The inhibited release of the TNF- $\alpha$  and IL-1 $\beta$  in the gingival crevicular fluid after compound treatment. The periodontitis rat model was constructed, afterwards treated by compound 1 or 2 at the consistence of 5 mg/kg. The ELISA was carried out to determine the TNF- $\alpha$  and IL-1 $\beta$  content in the gingival crevicular fluid.

# 3.3 Compound inhibited the release of the IL-1 $\beta$ and TNF- $\alpha$ in gingival crevicular fluid

In the former study, we have demonstrated the inhibitory effect of compounds on the relative expression level of the nf- $\kappa b$  and p53 in periodontal mucosal cells. In this experiment, this inhibitory activity of the compounds was further convinced by determining the content of TNF- $\alpha$  and IL-1 $\beta$  in the gingival crevicular fluid, which is the downstream production of the NF- $\kappa$ B-P53 pathway. From the results shown in Figure 5, we can find that the content levels of TNF- $\alpha$  and IL-1 $\beta$  in the group of the model were higher than those in a group of control. Different from compound 2, compound 1 could reduce the TNF- $\alpha$  and IL-1 $\beta$  in the gingival crevicular fluid and exert treatment activity on periodontitis. However, the related ligands and ions showed no effect on the content of TNF- $\alpha$  and IL-1 $\beta$  in the gingival crevicular fluid.

### 4 Conclusion

To sum up, we have triumphantly generated two novel mixed-ligand coordination polymers via adopting 2,5-thiophenedicarboxylate ( $H_2$ tdc) and bitopic flexible N-donor ligands 1,3-bis(1,2,4-triazol-1-yl)propane (btrp) or 1,4-bis((1H-benzo[d]imidazol-1-yl)methyl)benzene (bimb) as the organic building blocks. The two complexes were characterized via analysis of element, IR, thermal analysis and X-ray of powder diffraction. The structural determination shows that complex  $\bf 1$  is a two-dimensional layered

network which has a four-connected **sql** topology, complex **2** features a three-dimensional four-linked **sra** skeleton, and the symbol point is  $\{4^2,6^3,8\}$ . In the bioresearch, the protective function of compounds **1** and **2** against periodontitis were assessed, and the particular mechanism was discussed. The results of real-time RT-PCR exhibit that compound **1** has a stronger inhibitory effect on inflammatory response in periodontal mucosal cells than that of compound **2**. And the results of ELISA indicated that TNF- $\alpha$  and IL-1 $\beta$  contents in the gingival crevicular fluid was reduced by compound **1** significantly.

**Conflict of interest:** Authors declare no conflict of interest.

#### References

- [1] Furugen R, Kawasaki K, Kitamura M, Maeda T, Saito T, Hayashida H. Association of low fetuin-A levels with periodontitis in community-dwelling adults. J Oral Sci. 2020;62:67-9.
- [2] Voinescu I, Petre A, Burlibasa M, Oancea L. Evidence of connections between periodontitis and ischemic cardiac disease – an updated systematic review. Maedica. 2019;14:384–90.
- [3] Demkovych A. Effects of flavonol quercetin on activity of lipid peroxide oxidation in experimental bacterialimmune periodontitis. Interv Med Appl Sci. 2019;11: 55-0
- [4] Li X, Liu A, Du XD, Wang FX, Wang CC. Three silver coordination polymers constructed from 4,4'-bipyridine-like ligands and 2,5-thiophenedicarboxylic acid: crystal structures

- and photocatalytic performances. Transit Met Chem. 2019:44:311–9.
- [5] Rajak R, Saraf M, Mohammad A, Mobin SM. Design and construction of a ferrocene based inclined polycatenated Co-MOF for supercapacitor and dye adsorption applications. J Mater Chem A. 2017;5:17998-8011.
- [6] Zhang D, Gao B, Cui K. Modifying polysulfone into a bidentate Schiff base type macromolecular ligand and study on photoluminescence property of polymer-rare earth complexes of Eu(III) and Tb(III). J Polym Res. 2016;23:266.
- [7] Huang YR, Gao LL, Wang XQ, Fan LM, Hu TP. Syntheses, structures and luminescent properties of two novel Zn(II) coordination polymers. J Solid State Chem. 2018;258:854-8.
- [8] Rajasekhar B, Bodavarapu N, Sridevi M, Thamizhselvi G, RizhaNazar K, Padmanaban R, et al. Nonlinear optical and G-Quadruplex DNA stabilization properties of novel mixed ligand copper(II) complexes and coordination polymers: synthesis, structural characterization and computational studies. J Mol Struct. 2018;1156:690-9.
- [9] Voda I, Makhloufi G, Lozan V, Shova S, Heering C, Janiak C. Mixed-ligand cobalt, nickel and zinc coordination polymers based on flexible 1,4-bis((1H-imidazol-1-yl)methyl)benzene and rigid carboxylate linkers. Inorg Chim Acta. 2017;455: 118-31.
- [10] Rachuri Y, Subhagan S, Parmar B, Bisht KK, Suresh E. Selective and reversible adsorption of cationic dyes by mixed ligand Zn(II) coordination polymers synthesized by reactant ratio modulation. Dalton Trans. 2018;47:898–908.

- [11] Maity DK, Otake K, Ghosh S, Kitagawa H, Ghoshal D. Sulfonic group functionalized mixed ligand coordination polymers: synthesis, characterization, water sorption, and proton conduction studies. Inorg Chem. 2017;56:1581–90.
- [12] Lysova A, Samsonenko D, Dybtsev D, Fedin V. Synthesis and luminescence properties of new metal-organic frameworks based on zinc(II) ions and 2,5-thiophendicarboxylate ligands. Crystals. 2017;8:7.
- [13] Kang WC, Han C, Liu D, Cui GH. A bifunctional benzimidazole-based luminescent Zn(II) coordination polymer for detection of Hg<sup>2+</sup> and photocatalytic degrading of methylene blue. Inorg Chem Commun. 2019;106:81–5.
- [14] Guan BY, Kushima A, Yu L, Li S, Li J, Lou XWD. Coordination polymers derived general synthesis of multishelled mixed metal-oxide particles for hybrid supercapacitors. Adv Mater. 2017;29:1605902.
- [15] Balestri D, Costa D, Bacchi A, Carlucci L, Pelagatti P. Linker dependent dimensionality in Zn(II)-coordination polymers containing a flexible bis-pyridyl-bis-amide ligand. Polyhedron. 2018;153:278–85.
- [16] Croitor L, Coropceanu EB, Duca G, Siminel AV, Fonari MS. Nine Mn(II), Zn(II) and Cd(II) mixed-ligand coordination networks with rigid dicarboxylate and pyridine-*n*-aldoxime ligands: impact of the second ligand in the structures' dimensionality and solvent capacity. Polyhedron. 2017;129:9–21.
- [17] Zhu J, Luo J. Effects of entanglements and finite extensibility of polymer chains on the mechanical behavior of hydrogels. Acta Mech. 2018;229:1703–19.